The Quasar 1317+520: A Laboratory for Particle Acceleration

S.G. Jorstad and A.P. Marscher

Institute for Astrophysical Research, Boston University, 725 Commonwealth Ave., Boston, MA 02215, USA

Abstract. Multiwaveband images of extended jets in quasars reveal that in some locations electrons reach energies of at least 100 TeV, while in others the particle acceleration is less efficient. The jet of the quasar 1317+520 (z=1.06) contains shocks that are both transverse and oblique to the jet axis as well as regions where the axial magnetic field and polarization indicate cross-jet velocity shear. Strong X-ray emission turns on at the oblique shock, which is probably caused by the impact of an intergalactic cloud with the jet.

1. Introduction

The discovery of luminous X-ray jets in quasars by Chandra (e.g., Schwartz et al. 2000) has raised the question of the origin of the high energy emission at distances of hundreds of kiloparsecs from the central engine of an active galactic nucleus (AGN). The competing models involve one or two-zone models with the X-ray emission produced via either the synchrotron or inverse Compton mechanism. However, neither of the models can fully explain the observed properties of kiloparsec-scale jets (see Harris & Krawczynski 2006). Furthermore, the emission models only lightly address the ultimate problem of determining the processes by which particles can be accelerated to high energies (up to at least 100 TeV) in regions where the density and magnetic field are quite low. The answer is relevant not only to the jets of AGN, but also to the origin of very high-energy cosmic rays.

Significant progress in our understanding of jet physics can be achieved via multifrequency studies of jets that possess complex structure (multiple knots) detected at X-ray, optical, infrared, and radio wavelengths, as in the case of the quasar 3C 273 (Uchiyama et al. 2006). The detailed spectral energy distributions (SEDs) of bright features in the jet of this quasar reveal that optical synchrotron emission in the X-ray-bright knots is produced by a high-energy power-law component that is responsible for the X-ray emission as well. This high-E region occupies a smaller volume than does the radio synchrotron component that had previously been thought to be the site of the X-ray production via inverse Compton scattering of Doppler boosted cosmic microwave background photons (IC/CMB process). A possible cause of this frequency stratification is the presence of standing shocks in the jet that accelerate particles, which then propagate downstream as they lose energy to radiation and expansion (see Marscher & Gear 1985; Bai & Lee 2003) This model conforms with the extension of the radio emitting region downstream of the X-ray and optical knots. Such stationary shocks should be oblique to the jet axis if they are caused by

pressure mismatches with the surrounding medium or collisions with a cloud (e.g., Courant & Friedrichs 1948; Gómez et al. 1995). This geometry has the virtue of slowing down the jet flow only modestly, as opposed to the transverse shock ("working surface") near the end of the jet that slows the flow down to a subsonic speed, beyond which it forms an extended lobe.

The main processes by which particles are thought to be accelerated to ultra-high energies in the jets of AGN include:

1. Diffusive shock acceleration (e.g., Bell 1978; Jones 1994). Particles can reach very high energies if they pass across the shock front many times before they stream away from the front. It is highly controversial whether this is facilitated more by magnetic fields that are perpendicular, transverse, or oblique to the shock front.

2. Plasma turbulence induced by velocity shear (e.g., Stawarz & Ostrowski 2002; Rieger & Duffy 2004). Velocity shear across the jet should also lead to stretching of the magnetic field lines such that the net linear polarization is perpendicular to the jet axis, as is generally seen in quasar jets (e.g., Laing 1980).

Most likely, all variants of these processes occur in relativistic jets. There is no general agreement among theorists, however, as to either the efficiency of the processes in converting flow energy into relativistic particle energy or the upper limit to the electron energies that are reached in each variant mentioned above. The issue can, however, be settled observationally.

We have observed the quasar 1317+520 (z=1.06) with *Chandra*, the Spitzer Space Telescope (SST), and the Very Large Array (VLA). The data that we have collected thus far for this quasar reveal the presence of an oblique shock, a transverse shock, and regions with velocity shear in the knot $\sim 10''$ from the core where the X-ray, IR, and radio emission is detected. Here we discuss the physics of these features.

2.   Observations and Data Reduction

During Cycle 3 we obtained an 18 ksec exposure of the quasar 1317+520 with *Chandra* using ACIS-S3. We used version 3.4.0 of the CIAO software and the CALDB calibration database for the data analysis. We performed observations with the VLA at 15 GHz in B array on 2002 August 19, and at 5 GHz in A array on 2003 August 28. The data were edited and calibrated using the Astronomical Image Processing System (AIPS) software provided by NRAO. More recently, we observed the quasar with SST using IRAC at 4.5 and 8 μm with an exposure of 5.4 ksec. We used the European Southern Observatory image reduction software MIDAS to analyze the images. For the absolute flux calibration we followed the instructions of the Data Analysis Cookbook provided by the Spitzer Science Center as well as calibration procedures described by Reach et al. (2005).

The X-ray image (Fig. 1, *left*) reveals extended emission $\sim 10''$ from the core coinciding with the brightest radio feature ($C5$) of the multi-knot radio jet. The infrared images show a brightness enhancement at the position of knot $C5$ (Fig. 1, *right*).
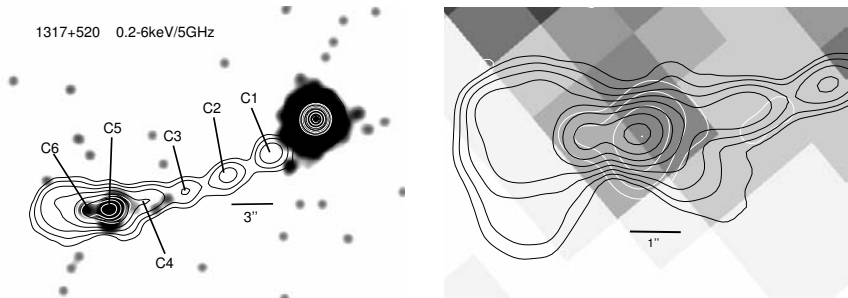
Figure 1.   *Left:* X-ray (grey scale) and radio (contours) images of 1317+520. The images are convolved with a circular Gaussian with FWHM=0.5″. The peak flux density of the radio image is 0.35 Jy/beam. *Right:* IR 4.5 μm (grey scale) image of knot $C5$ overlaid by radio (black) and X-ray (white) contours.

3.   Properties of the Radio Jet

The radio jet of the quasar has knotty structure and a well developed north-western lobe (Fig. 2). We have modeled the total and polarized intensity radio images with circular Gaussian components using the software Difmap and IDL. Table 1 contains the results of the modeling. Columns of Table 1 are as follows: (1) - name of component according to Figure 2; (2) - distance from the core; (3) - position angle with respect to the core; (4) - flux density at 5 GHz; (5) - spectral index between 5 and 15 GHz, $S_\nu \propto \nu^{-\alpha}$; (6) - degree of polarization at 5 GHz; (7) - position angle of polarization at 5 GHz.

Table 1.   Parameters of Jet Components

Component (1)	R'' (2)	Θ° (3)	S_{5GHz}, mJy (4)	α_r (5)	$p\%$ (6)	χ° (7)
Core	0.0	–	397±44	0.11±0.03	3.0±0.4	41±1
C1	2.5	125	5.8±0.6	0.57±0.03	29±3	41±1
C2	4.6	122	5.9±0.5	0.86±0.04	31±3	33±1
C3	6.5	118	4.4±0.5	0.94±0.04	32±4	24±1
C4	8.9	115	9.3±0.8	1.38±0.07	12±1	11±1
C5	10.0	113	79±6	0.75±0.02	19±2	9±1
C6	10.9	112	18±5	0.82±0.04	10±1	−66±2
C7	12.0	109	45±7	1.10±0.08	7±2	64±2
N1	7.7	−37	4.3±0.5	0.94±0.06	28±4	43±4
Lobe	17.5	−43	103±21	1.39±0.10	14±5	24±4

The parameters listed in Table 1 indicate that the degree of polarization in the jet within 7″ from the core is high, ∼30%, almost half of the maximum polarization for synchrotron radiation in a fully uniform magnetic field (Pachol-czyk 1970). The position angle of polarization is almost perpendicular to the jet direction, which implies that the magnetic field is aligned with the jet (the spectral indices of the knots confirm that the knots are optically thin). Figure
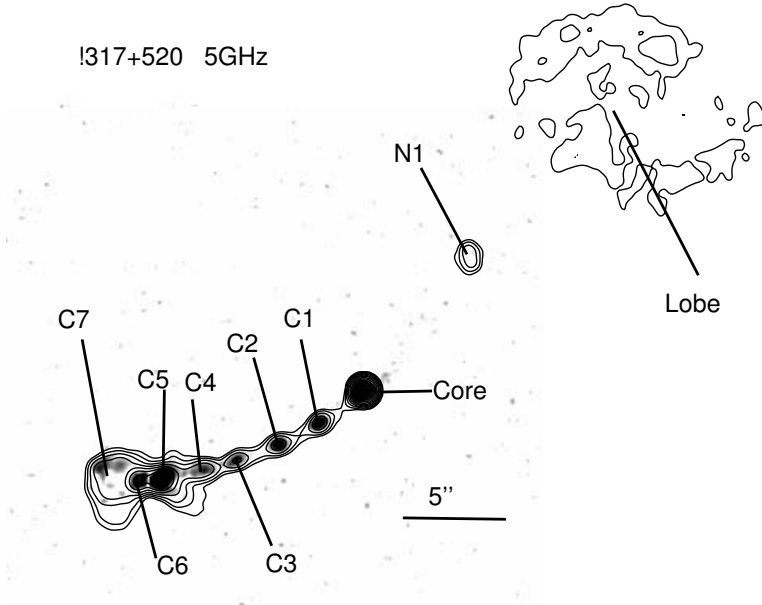
Figure 2.   Total (contours) and polarized (grey scale) intensity images at
5 GHz.

2 shows the presence of knot $N1$ on the counter-jet side of the image. If $N1$ is
really a counter-jet feature then we can estimate the ratio of jet to counter-jet
brightness, $J \approx 5.5$. If we assume that the source is intrinsically symmetric
(although there is some asymmetry between the jet and lobe alignment) then
$J = [(1 + \beta \cos \Theta_\circ / (1 - \beta \cos \Theta_\circ)]^b$ (Wardle & Aaron 1997), where β is the jet
flow speed in units of the speed of light, c, $\Theta_\circ$ is the viewing angle of the jet,
and $b = 3 + 2\alpha$ in the case of the jet with well-ordered magnetic field along the
velocity vector. This gives the estimate $\beta \cos \Theta_\circ \sim 0.19$.

The parsec-scale jet direction of the quasar (Aars & Hough 2005) coincides
with that of $C1$ and $C2$ on kiloparsec scales. By comparing the position of a
bright knot in the 1992 VLBI map at 5 GHz from the CJ1 survey with that in
the 2002 VLBA image at 8.4 GHz by Aars & Hough (2005), we have tenta-
tively estimated the apparent speed in the jet to be $\beta_{app} \sim 5.7$, which implies
a bulk Lorentz factor $\Gamma \geq 5.7$. The superluminal motion is inconsistent with
the jet-counterjet flux ratio. This implies deceleration of the jet from parsec to
kiloparsec scales if the tentative proper motion is correct.

Table 1 indicates that the spectral index steepens with distance from the
core but flattens in knot $C5$. The polarization in the 5 GHz image reveals
complex magnetic field structure in the $C4$-$C6$ region (Fig. 3). The image
shows a billowy counterlobe (seen in Fig. 2) but only modest flaring of the
structure at the end of the jet side beyond knot $C6$, which has the properties of
a working surface (shock and magnetic field transverse to the jet axis - Fig. 3,
region A). There is also a transverse extension of the emission to the southwest

of $C5$. Taken together, these features suggest that a giant cloud is colliding with the jet from the northeast, with ram pressure confining the region east of the working surface and pushing some of the jet material (probably from the edges) to the southwest of $C5$. Such an interaction of a gaseous structure with the jet flow should lead to the formation of an oblique shock in the jet. Indeed, in the northern half of $C5$ the magnetic field is oriented at a substantial angle to the jet axis (Fig. 3, region B), as expected for an oblique shock, which amplifies the component of the field that is parallel to the shock front. The magnetic field in the southern half of $C5$, on the other hand, is very well ordered and parallel to the flow direction eastward of $C5$ (Fig. 3, region C), suggestive of velocity shear that stretches the field lines. Such velocity shear must be present where the jet bends.
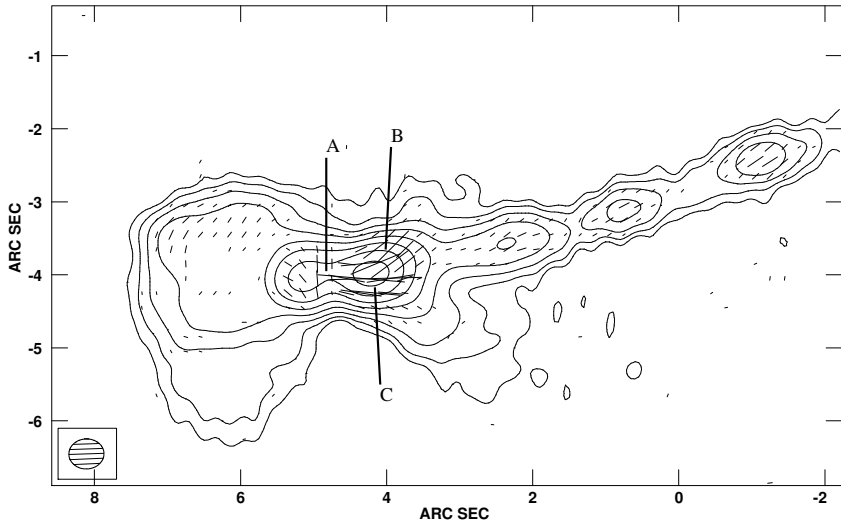

Figure 3. The magnetic field structure in the jet of 1317+520 (black linear segments within total intensity contours). Letters designate regions with different processes in the jet: A - transverse shock, B - oblique shock, and C - velocity shear stretching of field lines.

4. Spectral Energy Distribution of Knot C5

The current data do not allow us to construct the spectral energy distributions (SEDs) separately for regions A, B, and C that would produce the most reliable estimate of the efficiency for the different processes of particle acceleration. Here we present the SED of the whole complex that we associate with the brightest feature $C5$. The feature was detected at radio, IR, and X-ray wavelengths (see Fig. 1). We measure the flux densities and spectral indices of $C5$. The spectral

indices at high frequencies are as follows: $\alpha_{IR} = 0.96 \pm 0.11$ and $\alpha_X = 0.75 \pm 0.25$. Figure 4 (*top*) shows the observed SED of the knot $C5$, where $\epsilon = h\nu/(mc^2)$.
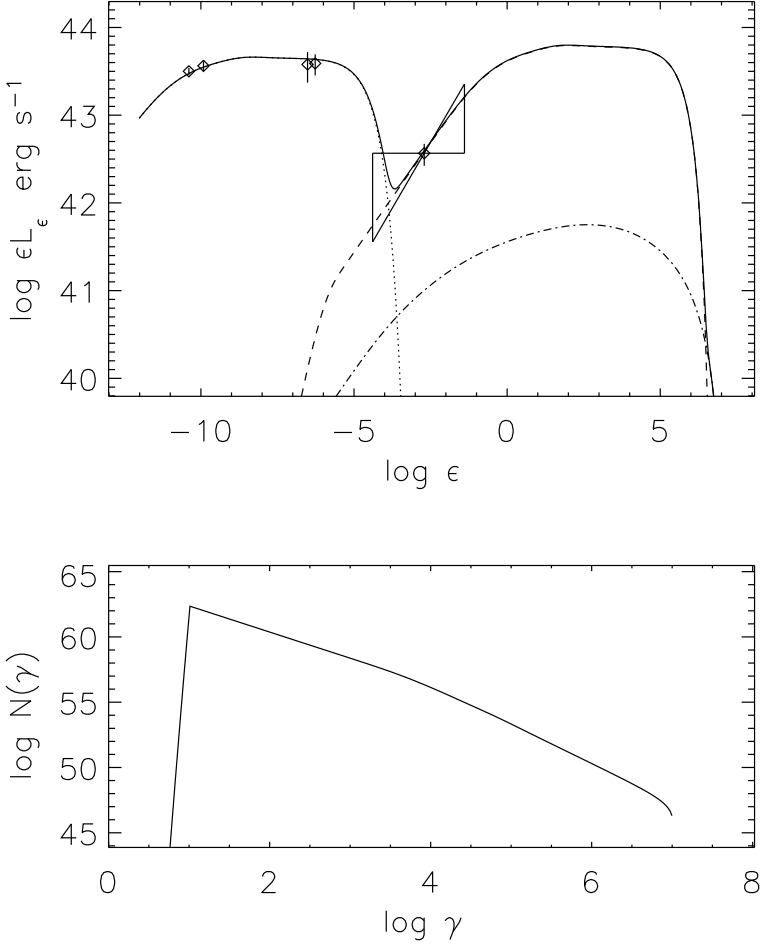

Figure 4.   *Top:* Observed SED for knot $C5$ (diamonds); curves represent simulated SEDs for synchrotron (dotted), EC/CMB (dashed), and SSC (dash-dotted) mechanisms; the solid line is the sum of all three processes. *Bottom:* The energy distribution of the relativistic electron population.

We employed the code developed by Markos Georganopoulos to sumulate the SED. The code calculates the synchrotron, synchrotron-self-Compton (SSC),

and inverse Compton (IC) from external photons (EC) emission of a sphere with a magnetic field. The sphere moves with a constant Lorenz factor through an external photon field. An electron distribution with a power law is continuously injected throughout the sphere. Synchrotron and IC losses are taken into account and the electrons can escape from the sphere. The emission is calculated when the system reaches a steady-state. Figure 4 shows simulated SEDs that give the best fit to the observed SED. Agreement is achieved with the following initial parameters: $\Gamma = 1.2$, $\delta = 1.2$, $m = 1 + \alpha = 2$, $\gamma_{min} = 10$, $\gamma_{max} = 10^7$, $L_{com} = 2 \times 10^{46}$ erg/s, $B = 15$ μG, r=18 kpc, t_{esc}=5, and the external field is the Cosmic Microwave Background (CMB). Here γ_{min} and γ_{max} are the minimum and maximum Lorentz factors of the electrons, respectively (the energy distribution for the electrons is shown in Fig. 4, *bottom*), m is the photon spectral index, L_{com} is the comoving luminosity injected into the sphere, B is the magnetic field, r is the radius of the sphere, and t_{esc} is the electron escape time in units of r/c.

The results of the simulations show that in the case of a single population of electrons, the X-ray emission is produced via the EC/CMB mechanism, even though the bulk Lorentz factor is rather low (Γ decreases from parsec to kiloparsec scales by a factor of $\sim$5). With the derived value of the high energy cutoff to electron distribution and the low magnetic field, the electrons are unable to produce synchrotron X-rays owing to radiative losses, which cool the electrons before they can escape from the region. The region posseses similar energy in the magnetic field, $U_B = 8.6 \times 10^{-12}$ erg/cm^3, and in the particles, $U_p = 5.3 \times 10^{-12}$ erg/cm^3 as expected for energy equipartition. The detection of the synchrotron IR and EC/CMB X-ray (if it is correct) emission suggests an enhancement of electrons with $\gamma \sim 1000$ in the $C5$ region compared with the relativistic electron population in knots $C1$-$C4$, in which X-ray emission is not detected. The IR measurements in knots $C1$ and $C2$ are very noisy due to large uncertainties in the PSF near the core. However, the IR estimates for knot $C4$ and the upper limit for $C3$ imply a high energy cut-off of the population of relativistic electrons $\gamma_{max} \leq 7 \times 10^5$ in these knots. This suggests that the oblique shock in the northern section of $C5$ and shear region in its southern section most likely create an additional component that widens the electron distribution in $C5$ up to $\gamma_{max} \sim 10^7$. Moreover, such a high value of γ_{max} and the EC/CMB origin of the X-ray emission in $C5$ imply that the region is a source of γ-ray emission, which could be detected with GLAST if the core of the quasar is not a bright γ-ray emitter.

5. Conclusion

Chandra surveys of quasars (Sambruna et al. 2004; Marshall et al. 2005) reveal that the majority of radio-loud quasars possess extended X-ray emission on kiloparsec scales. The origin of this emission is still hotly debated. Multi-frequency deep imaging at X-ray, optical, IR, and radio wavelengths along with accurate spectral indices in each band and polarization observations are required to understand the phenomenon. The suggested EC/CMB origin of the X-ray emission on kiloparsec scales (e.g., Tavecchio et al. 2000) can be tested via GLAST monitoring of non-EGRET quasars with detected kiloparsec scale X-ray

emission. The high sensitivity of GLAST might be sufficient to measure γ-rays produced via EC/CMB along with the X-ray emission. Such γ-ray emission should not show variablity, in contrast to γ-ray emission from the nuclei of the EGRET-detected blazars.

References

Aars, C. E., & Hough, D. H. 2005, ASP Conf. Series, 340, 162
Bai, J. M., & Lee, M. G. 2003, ApJ, 585, L113
Bell, A. R. 1978, MNRAS, 182, 143
Courant, R., & Friedrichs, K. O. 1948, Supersonic Flow and Shock Waves (Springer-Verlag)
Gómez, J. L. 1995, ApJ, 449, L19
Harris, D. E., & Krawczynski, H. 2006, ARA&A, 44, 463
Jones, F. C. 1994, ApJS, 90, 561
Laing, R. A. 1980, MNRAS, 193, 439
Marshall, H. L., et al. 2005, ApJS, 156, 13
Marscher, A. P., & Gear, W. K 1985, ApJ, 298, 114
Pacholczyk, A. G. 1970, Radio Astrophysics (San Francisco: W.H. Freeman)
Reach, W. T., et al. 2005, PASP, 117, 978
Rieger, F. M., & Duffy, P. 2004, ApJ, 617, 155
Sambruna, R., et al. 2004, ApJ, 608, 698
Schwartz, D. A., et al. 2000, ApJ, 540, L69
Stawarz, L., & Ostrowski, M. 2002, ApJ, 578, 763
Tavecchio, R., et al. 2000, ApJ, 544, L23
Uchiyama, Y., et al. 2006, ApJ, 648, 910
Wardle, J. F. C., & Aaron, S. E. 1997, MNRAS, 286, 425